Solid-State Electronics 192 (2022) 108259

Contents lists available at ScienceDirect

Solid State Electronics

journal homepage: www.elsevier.com/locate/sse

Improved inter-device variability in graphene liquid gate sensors by laser treatment

Jorge Ávila [*,1], Jose C. Galdon [1], Maria-Isabel Recio, Norberto Salazar, Carlos Navarro, Carlos Marquez [*], Francisco Gamiz

Nanoelectronics Research Group (CITIC-UGR), Department of Electronics, University of Granada, 18071 Granada, Spain

ARTICLE INFO

Keywords:
Graphene
Laser treatment
Biosensors
Sensors

ABSTRACT

We investigate the influence of a visible laser treatment on the electrical performance of CVD-grown graphene-based liquid gate sensors. This method allows us to treat locally the graphene sheet, improving the performance of the structure for biochemical sensing applications. It was found critical to control the atmosphere in which the laser treatment takes place. An optimized ambient-air laser exposure shifted the Dirac point (minimum of the conductivity voltage) around 300 mV to lower voltages, together with a decrease of the inter-device electrical variability. These results open the door to use the laser treatment to increase the sensibility and reproducibility of liquid gate graphene-based devices as sensors or biosensors.

1. Introduction

Graphene, a monolayer of carbon atoms packed into a two-dimensional honeycomb lattice, has received an exceptional attention due to its excellent electrical, optical, thermal and bendability properties [1–3]. In addition, graphene is very sensitive to changes in the surroundings while its reduced thickness improves the electrostatic control of the channel, thus making it particularly attractive for sensing applications [4]. There are several examples of recent studies about graphene-based sensors and biosensors in different perspectives [5–7], for example, for the detection of biomarkers[8] or heavy metals [9]. However, in the case of biosensors, they should operate at or near physiological conditions, so it is essential to use graphene in aqueous solutions. Electrochemical studies have shown that the ions accumulate at the surface of graphene when a gate voltage is applied between the electrodes, without charge transferred across the interface [10]. These studies suggest that graphene operates nearly as an ideal polarizable electrode [11,12]. The graphene–electrolyte interface is typically modeled as an electrical double layer capacitance (EDLC), constituted by two layers of ions that are created at the surface of graphene. The first layer is composed of ions of opposite charges to those present in the graphene, and the second layer is composed of positive and negative charged ions that progressively reach the potential of the solution far from the graphene surface. The EDLC can be modulated applying a voltage at a reference electrode immersed in the electrolyte solution, controlling the number of free carriers in graphene, and therefore its conductivity. The minimum of free carriers, and thus the minimum of conductivity, is reached when the valence and the conduction band meet at a point called the Dirac point, the gate bias at which the Fermi level reaches the Dirac point is the charge neutrality point or Dirac voltage.

Electrochemical gated graphene sensors employing electrolytes such as ionic liquids and aqueous solutions have been extensively reported, showing excellent performances [13,14]. Nonetheless, due to the high sensitivity of graphene and the complex nature of the electrolyte solutions, the reproducibility among devices can be challenging. For example, some factors that affect the inter-device variability are the different doping levels of the graphene sheet due to graphene–substrate interactions or fabrication residues [15]. Moreover, the presence of interface states, traps and mobile charges also affects the sensing capability of the fabricated devices. There are studies showing important variations in the Dirac voltages from −5 to 2 V in a series of 25 devices [16], or from 0 to 8 V in a series of 7 devices [17]. In both cases, the graphene was grown by CVD. It is crucial to explore different strategies to reduce this variability in order to achieve more homogenous inter-device electrical properties. Different strategies have been explored in order to remove any potential residue and improve the quality of the graphene sheet, as thermal annealing, plasma, UV–vis light, electrical or mechanical treatments [18]. One of the most popular strategies has been

* Corresponding authors.
E-mail addresses: jorgeavila@ugr.es (J. Ávila), carlosmg@ugr.es (C. Marquez).
[1] These authors contributed equally to this work.

https://doi.org/10.1016/j.sse.2022.108259
Received 8 November 2021; Received in revised form 30 January 2022; Accepted 21 February 2022
Available online 25 February 2022
0038-1101/© 2022 The Authors. Published by Elsevier Ltd. This is an open access article under the CC BY-NC-ND license (http://creativecommons.org/licenses/by-nc-nd/4.0/).

the laser processing of the graphene layer. Not only to improve the quality of the graphene sheet but for the in situ fabrication of graphene in different substrates, like polyimide. Here, graphene has found a wide range of applications of electronic devices, with the advantage of a flexible substrate, as supercapacitors, optoelectronic devices, sensors, and actuators[19–21].

In this work, we have explored the effect of the irradiation of the graphene layer using a visible laser as a straightforward and rapid treatment to improve the inter-device electrical variability in graphene-based liquid gate sensors. We have also studied the influence of the atmosphere during this laser treatment, finding significant differences if the irradiation is performed in ambient atmosphere or under vacuum conditions. This strategy can modify locally the graphene surface without compromising the rest of the device, being useful if sensible materials are presented and avoiding damage in the contacts. By employing this method, we have observed a reduced Dirac voltage and an improved inter-device electrical variability in graphene-based sensors.

2. Experimental Setup

Graphene was synthesized through low-pressure chemical vapor deposition (LPCVD) where polycrystalline copper foil was used as catalytic substrate. The reaction was made at 1 Torr using methane (CH_4) as a carbon precursor. The foils were first heated up to 1000 °C in a hydrogen (H_2) environment to reduce the native copper oxide on the copper foil surface. Then, a H_2/CH_4 gas mixture (50 sccm: 30 sccm) was added during the graphene growth at 1000 °C for 30 min. The cooling down step was made by opening the furnace, during which the gas composition was remained the same. Later, the graphene layers were transferred to cleaned quartz substrates using the PMMA based technique [22]. In this method, a Poly(methyl 2-methylpropenoate) (PMMA) solution, dissolved in anisole, was spin coated on top of the graphene films at 2000 rpm for 1 min. After coating, the samples were annealed at 80 °C for 10 min. Then, the samples were immersed in ferric chloride for 30 min to etch the copper. The resulting PMMA/graphene films were floated on the surface of the solution. The suspended films were rinsed three times with deionized water followed by hydrochloric acid (10%) and deionized water again to remove any residual copper etchant. Finally, the graphene/PMMA stacks were transferred to cleaned quartz substrates. The PMMA film was removed with an acetone bath at 105 °C for 20 min. After that, the samples were washed with isopropanol and dried with nitrogen. In order to remove any PMMA residues and clean the graphene surface, the samples were annealed in a furnace at 300 °C in an Ar/H_2 atmosphere for 1 h.

The sensor fabrication process is illustrated in Fig. 1: After the graphene deposition, reactive-ion etching (RIE) at 10 W and 30 sccm of O_2 was used to pattern the graphene employing a solid mask. Up to six sensors were fabricated on each substrate. Then, the Cr (5 nm)/Au (100 nm) electrodes were deposited by physical vapor deposition. Finally, the laser treatment was performed on the graphene layer using a computer-controlled laser engraver (Laserbot from Makeblock) equipped with a blue diode laser (Makeblock). The laser wavelength is 445 nm (blue) and the maximum light power is 1.3 W. For the laser treatment, the laser power was set to 25% with respect to the maximum power. The spot size is 100 μm, and it is assumed that the energy is distributed evenly in all the area. The focus distance is adjustable by the laser module itself and it was fixed at 5 centimeters, the sample is placed at that point, without any modification of the optical path. One cycle of laser treatment consists of irradiation with the laser of the full graphene surface. To do that, the area to be irradiated is programmed in the engraver software, and it will automatically control the movement of the

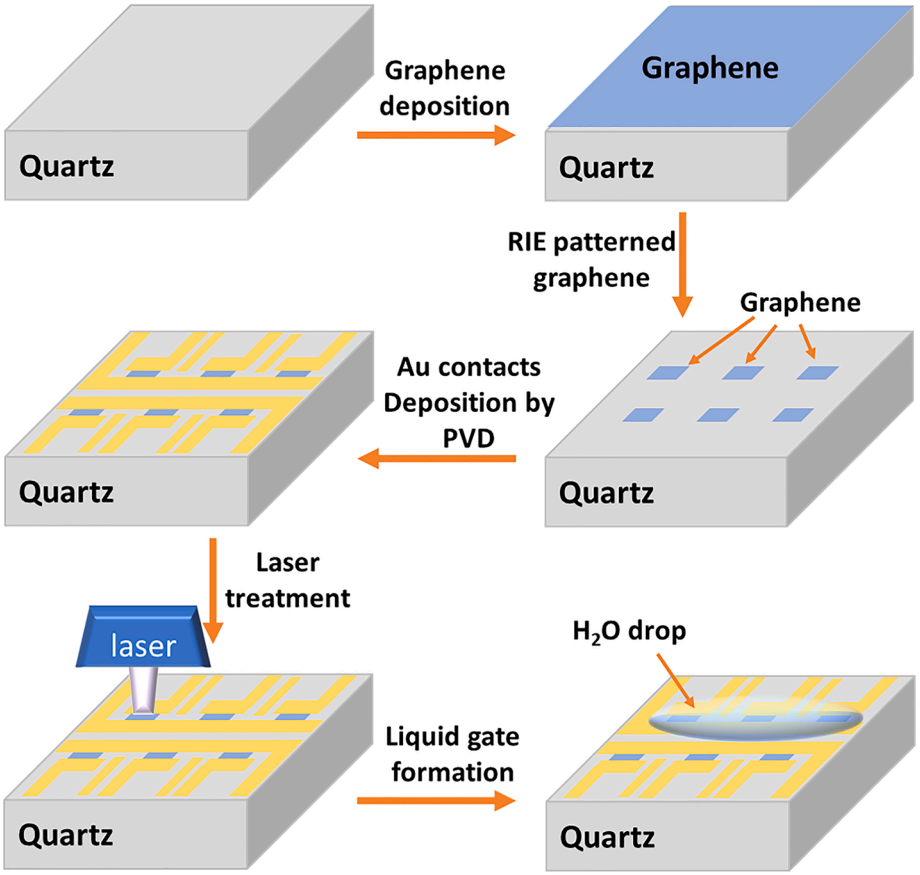

Fig. 1. Scheme of the fabrication flow of the liquid gate graphene devices, including the laser treatment.

laser to irradiate the desired surface. The laser treatment was performed in two different atmospheres, in ambient air or in vacuum. In the case of the vacuum atmosphere, the sample was placed inside a closed steel container, with a quartz window through where the laser was shone, at an approximate pressure of 10^{-2}-10^{-3} torr.

To evaluate the electrochemical characteristics of the devices, a phosphate buffered saline solution (PBS) at a 1X concentration, was placed covering the graphene to perform the liquid gate. PBS is a buffer solution commonly used in biochemical research, as the osmolarity and ion concentrations of the solutions match those of the human body. Hence, using this buffer solution, we evaluate the sensor in near human physiological conditions. Raman spectra were acquired using a Confocal Micro-Raman system (JASCO NRS-5100) with a 532 nm excitation source. The laser power was kept below 1 mW to avoid damage or heating with 100 × objective giving a laser spot size of about 1 μm. XPS was performed using a Kratos Axis Ultra-DLD spectrometer with Al Kα (1486.6 eV) radiation. The static DC characteristics were acquired using a Keithley SCS 4200 and an Agilent B1500 systems. The low-frequency noise characterization was carried out using a low-noise-current amplifier connected to a software-based spectrum analyzer [23].

3. Results and Discussion

Before considering the double layer capacitance effect in the devices, the laser radiation on the graphene sheet was evaluated in Fig. 2.

The graphene layer resistance was measured, without a liquid gate, at a fixed drain-source voltage ($V_D = 0.1\,V$) after each laser exposure (Fig. 2). A growth in the resistance of the devices was observed for both atmospheres with each laser exposure iteration. In the case of the sample treated in ambient air (Fig. 2.a), the increase in the resistance slows down with the number of laser cycles, saturating after 6 to 8 cycles. In contrast, for the sample irradiated under vacuum (Fig. 2.b), we observe a constant increase of the resistance that continues growing after more than 10 laser cycles. These results show that the atmosphere in which the laser treatment takes place can have an important effect on the electrical properties of the graphene sheet.

In order to evaluate the structural repercussion of the laser irradiation on the graphene sheet, Raman spectroscopy and X-ray photoelectron spectroscopy (XPS) analysis were carried out before and after the laser treatments (Fig. 3). The Raman spectra of the graphene layers are presented in Fig. 3.a. Prior to laser exposure, the Raman spectrum of the graphene device shows the signature for pristine single-layer graphene, with a G peak at ≈1590 cm^{-1} and a 2D peak at ≈2680 cm^{-1}, together with the presence of a small D peak at ≈1340 cm^{-1}. After the laser treatment in vacuum, the spectrum of the graphene layer is kept practically unchanged, without any significant variation of the intensity of the peaks and without the inclusion of any new feature. However, when the graphene is treated in ambient air, a noticeable increase of the D peak is observed, as well as the emergence of the D' peak (≈1620 cm^{-1}).

These results corroborate that each kind of laser treatments have different effects on the structural order of the graphene. On the one hand, the electrical implications of the laser treatment in vacuum on the graphene are not reflected on the Raman spectrum, hence it is not clarifying the origin of the increase in the resistance. While in the case of the treatment in ambient air, the increase of the D peaks are clearly pointing to an alteration in the structure that can be linked to the formation of new defects. The emergence of the D' peak is often related to the formation of sp^3-type defects [24–27]. These new defects have an adverse impact on the electrical behavior, increasing the graphene resistance. Nevertheless, the resistance stabilized at higher number of laser treatments, indicating that possibly the effect of the laser in the graphene structure saturates. A possible explanation is that these defects are formed mainly in the grain boundaries, where dangling bonds are receiving enough energy to react with the ambient atmosphere, generating some oxide species [28]. These species would hinder the electric

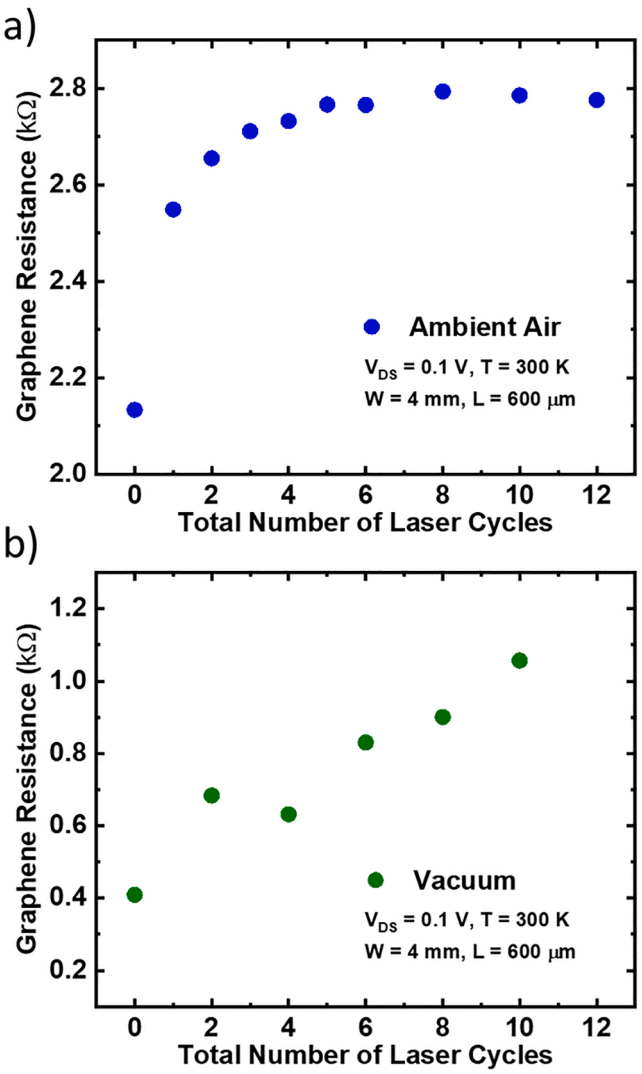

Fig. 2. The graphene device resistance measured at 0.1 V drain-source bias without liquid gate for different numbers of laser cycles performed a) in ambient air and b) under vacuum condition.

transport between grains, increasing the electric resistance. Despite deteriorating the sheet resistance of the graphene layers, these defects may have different implications when the graphene-electrolyte interface is formed.

To clarify the effect of the defects on the graphene characteristics and its origin, we have studied the XPS spectra of the graphene sheets on copper (without any transfer), and after it is transferred onto quartz substrates. This study allows us to discard any possible implication of the PMMA and the transfer process on the resistance results. In Fig. 3.b, the XPS wide spectra of graphene before any laser treatment are presented. In the spectrum of the graphene on copper, we observe the expected peaks for carbon, oxygen and copper. While in the XPS spectrum of the graphene transferred on quartz, the copper peak is absent, as presumed, and the silicon peak coming from the substrate is observed. Also, we can notice the presence of the iron peak coming from copper etchant ($FeCl_3$) residues that have not been completely removed. In the sample measured on copper, we determine a proportion of around 5 carbon atoms per oxygen atom, being similar before and after the laser treatments. This concentration could be higher if we take into account that the copper surface can be oxidized in some degree. This proportion of oxygen in the sample is high for a pure graphene layer. However, we can consider that the origin of the majority of the oxygen atoms are

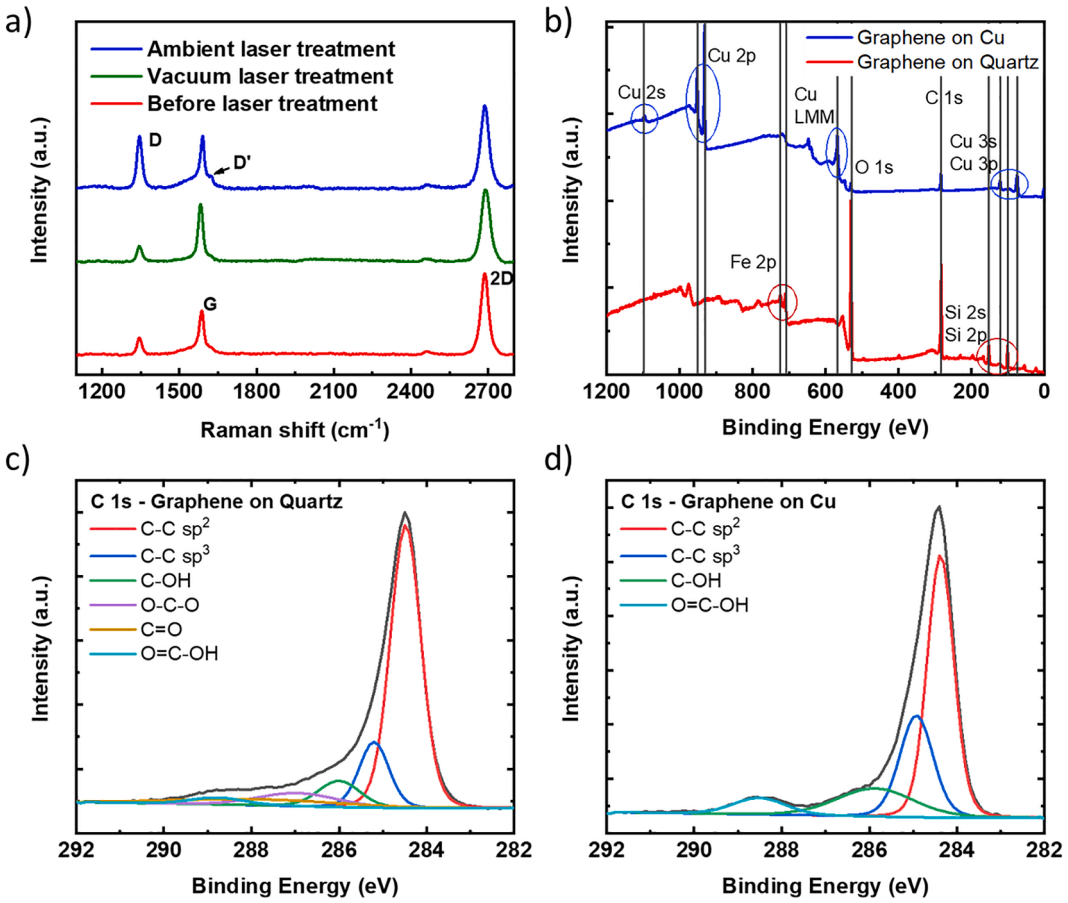

Fig. 3. a) The graphene Raman spectra before and after the different kind of laser treatments. The Raman laser wavelength is 532 nm. b) Comparison of the XPS wide spectra for the graphene on copper and after the transfer on quartz. c) XPS spectrum of the C1s peak for the graphene on copper. d) XPS spectrum of the C1s peak for the graphene transferred on copper.

superficial contaminants deposited during the sample manipulation. Nevertheless, this gives us a baseline value of reference for the amount of oxygen contamination that a sample can have. In the sample measured on quartz, the amount of oxygen detected is higher, but the signal is mainly proceeding from the oxygen in the SiO_2 substrate. By deducting the signal coming from the substrate, we observe a proportion of around 4 to 5 carbon atoms per oxygen atom. This value means that after the sample preparation there is not an important variation in the sample composition, only maybe a slight increase of the amount of contaminants deposited on the top surface.

To better understand the carbon composition of the samples, we have studied the components in the C 1s spectra (Fig. 3.c and 3.d). The main peak at 284.4 eV is assigned to the C–C sp^2 bonds, and the peak at 285 eV to the C–C sp^3 bonds. The rest of the components are assigned to the different kind of carbon–oxygen bonds. The component at 286 eV is assigned to C atoms directly bonded to oxygen in hydroxyl configurations (C-OH). At 286.8 eV, the component is attributed to epoxide group (C-O-C). And the two smaller components at higher energies (287.8 and 288.9 eV) to the carbonyl (C = O) and carboxyl (COOH) groups. In Fig. 3.c, we observe in the deconvolution of the graphene spectrum on quartz a wider variety of component than in the spectrum on copper (Fig. 3.d). These changes in the composition are taking place after the transfer of the graphene sheet and can be related to PMMA residues or similar contaminants.

The comparison of the different components for the case of graphene on quartz can be found in Table 1, also including the influence of the laser treatment in both atmospheres. The amount of C-O bonds follows the same proportion as in the wide XPS spectra, with a 25% of oxygen bonds. Analyzing the influence of the laser treatments in the composition, we can detect an increase of the sp^3 together with a decrease of the sp^2 component for the graphene layer when the layer is treated in ambient air. The increase of the C–C sp^3 is in agreement with the Raman interpretation, where the rise of the D peaks could be related to the formation of sp^3-type defects. On the other hand, the graphene layer treated in vacuum has a higher sp^2 and a reduced C-O component. Therefore, the composition of the graphene layer after the treatment in vacuum can be identified as less defective.

Table 1
Comparison of the C 1s XPS composition of graphene layers on copper and quartz, before and after the different kind of laser treatments.

	Quartz Ambient Laser		Quartz Vacuum Laser		Quartz Before Laser	
	Position (eV)	Area (%)	Position (eV)	Area (%)	Position (eV)	Area (%)
C-C sp^2	284.5	58.7	284.6	61.5	284.4	60.1
C-C sp^3	285.2	15.1	285.2	13.8	285.2	13.8
C-O	286-289	26.2	286-289	24.7	286-289	26.1

After the deposition of the liquid gate and the formation of the electrical double layer capacitance, we measured the transfer characteristic ($R = V_D/I_D$) of a device using two different metals as the gate electrode (Fig. 4.a). A proper modulation of the resistance as a function of the liquid gate voltage is observed, together with a shift of the Dirac point depending on the metal electrode. This shift from 0.83 V (gold) to

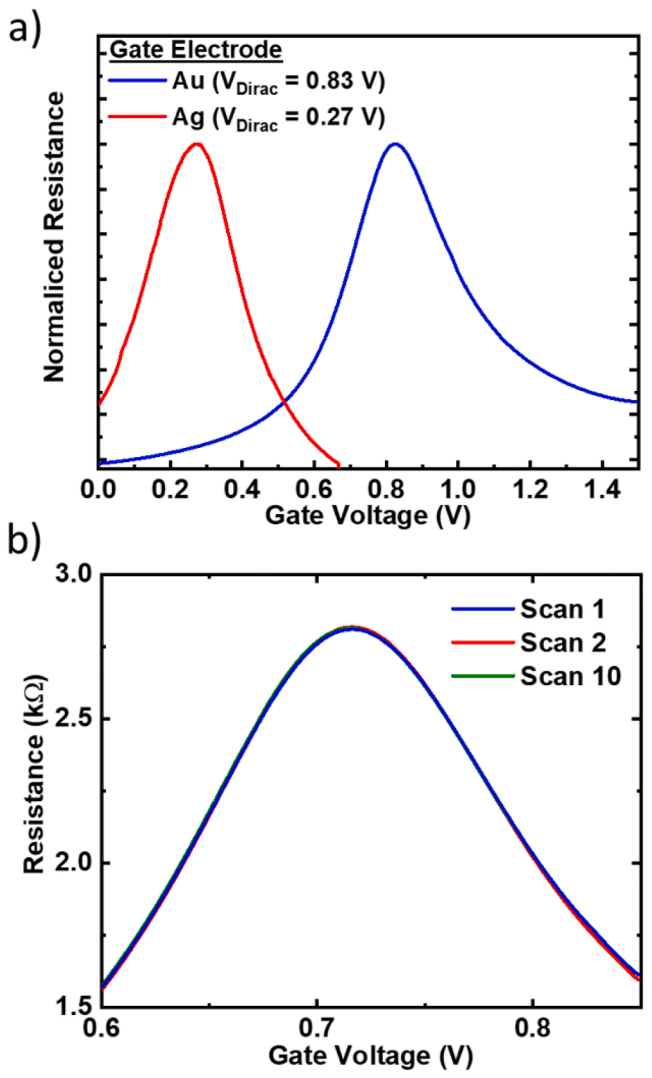

Fig. 4. a) Resistance versus gate voltage characteristic curves for a device measured employing gold(blue line) or silver (red line) as the gate electrode. The drain source bias was set at 0.1 V. The Dirac voltage is defined as the voltage when the resistance reaches the maximum. b) Resistance versus gate voltage characteristic curves for a device measured up to 10 times to evaluate its stability. The curves are almost completely overlapping.

0.27 V (silver) is mainly due to the difference in the work function of the employed metal. In order to work in aqueous solutions, low voltages are desirable to keep the working conditions below the water electrolysis potential (1.2 V), avoiding secondary reactions and keeping a low gate-drain current [29]. The lower Dirac voltage for the silver gate electrode can be interesting for low energy consumption applications. However, silver can easily be oxidized in contact with the aqueous solution. Hence, it is preferable the use of a gold electrode as a more electrochemical stable option despite the higher voltages. In the following devices, gold is used as the gate electrode. In Fig. 4.b we can see the resistance versus gate voltage characteristic curves for a device measured several times in the same conditions to evaluate its stability. We can observe that after 10 measurements the curve is still similar to the first one without any important variation in the consecutive measurements.

Fig. 5 shows the transfer characteristics of two devices when using the liquid gate for successive laser treatment cycles in ambient air (Fig. 5.a) and vacuum (Fig. 5.b). Note that in both cases, there is a modulation of the channel conductivity as a function of the liquid gate voltage. In the case of the device treated in ambient air (Fig. 5.a), the device resistance initially decreases with the successive laser cycles, but after 4 cycles it starts to saturate. At the same time, the Dirac point shifts to lower voltages from 1 V before the laser treatment, down to 0.66 V after 8 cycles (Fig. 5.c). Then, at higher number of laser cycles, the rise of the resistance is accelerated and the Dirac voltage shifts to higher voltages. This indicates that a high number of laser cycles is drastically damaging the sensor.

In the case of the device irradiated under vacuum conditions (Fig. 5. b), the Dirac point shifts to lower voltages from around 1.1 V down to 0.8 V after 10 laser cycles (Fig. 5.c), while the device resistance was kept approximately at the same range. In contrast with the device treated in ambient air (Fig. 5.a), there is not an increase in the resistance at high number of laser cycles, indicating that the laser treatment under vacuum is not significantly damaging the device. However, at high number of laser cycles, the Dirac point shift behaves erratic, and the curves become broader, indicating a slightly harmful effect.

Fig. 5.d shows a comparison of the Dirac voltages distribution of a series of devices without any laser irradiation and processed with the two types of laser treatment for a total number of four laser cycles. The devices treated in ambient air show significant reduction of the electrical inter-device variability. The standard deviation is reduced from 120 down to 24 mV, together with an improved average Dirac voltage of 810 mV. However, for the devices treated in vacuum, there are no significant differences comparing with the devices as-synthesized (without any laser treatment). A standard deviation of 110 mV and an average Dirac voltage of 920 mV for the case of the laser treatment at vacuum conditions, versus an average Dirac voltage of 950 mV and a standard deviation of 120 mV for the case without laser treatment. These results are in agreement with the structural characterization previously discussed. The devices treated in vacuum present a similar structural composition to the devices before any treatment, and the electrical behavior is comparable or slightly improved. However, the devices treated under ambient air conditions present a deterioration of the electrical performance after the laser exposure. Nonetheless, at low number of laser cycles, the sensing capabilities are improved with a lower resistance and with a reduction of the Dirac voltages compared to the device without laser treatment. Note that the inter-device variability is a critical constraint for sensing applications. This variability improvement could reside in a laser-induced transformation of the graphene structure. Induced defects and oxidized species at grain boundaries can improve the electrical double layer capacitance, which finally improves the liquid gate/interface, making it more reliable for sensing and less variable among devices [30,31].

Low-frequency noise characterization may shed light on the defect implications in these graphene sensors before and after the laser irradiation. As Fig. 6 shows, the graphene layer presents a normalized power spectral density (PSD) of the noise formed by a flicker or 1decade/1decade (1/f) contribution at low frequency and a Lorentzian contribution with center frequency around 10^4 Hz. This result indicates that graphene sheets are affected by carrier number fluctuations at low frequencies and by capture and emission processes of carriers at higher frequencies [32]. According to the similar spectrum observed before and after the laser irradiation (regardless in vacuum or air ambient conditions), these fluctuations are not enhanced by the laser treatment, suggesting a graphene resistance increased without a degradation of the interface after the laser exposure. This result means that, despite the increase of the defects discussed in the structural characterization and the conductivity degradation observed in the direct-current characterization, once the double layer is formed, these defects do not imply an increase in the spectral density of the current.

4. Conclusion

Main parameters for using graphene liquid-gate devices as sensors have been evaluated before and after employing a laser treatment in ambient air and vacuum conditions. Despite presenting a slight increase in the graphene resistance after the laser exposure in ambient condition,

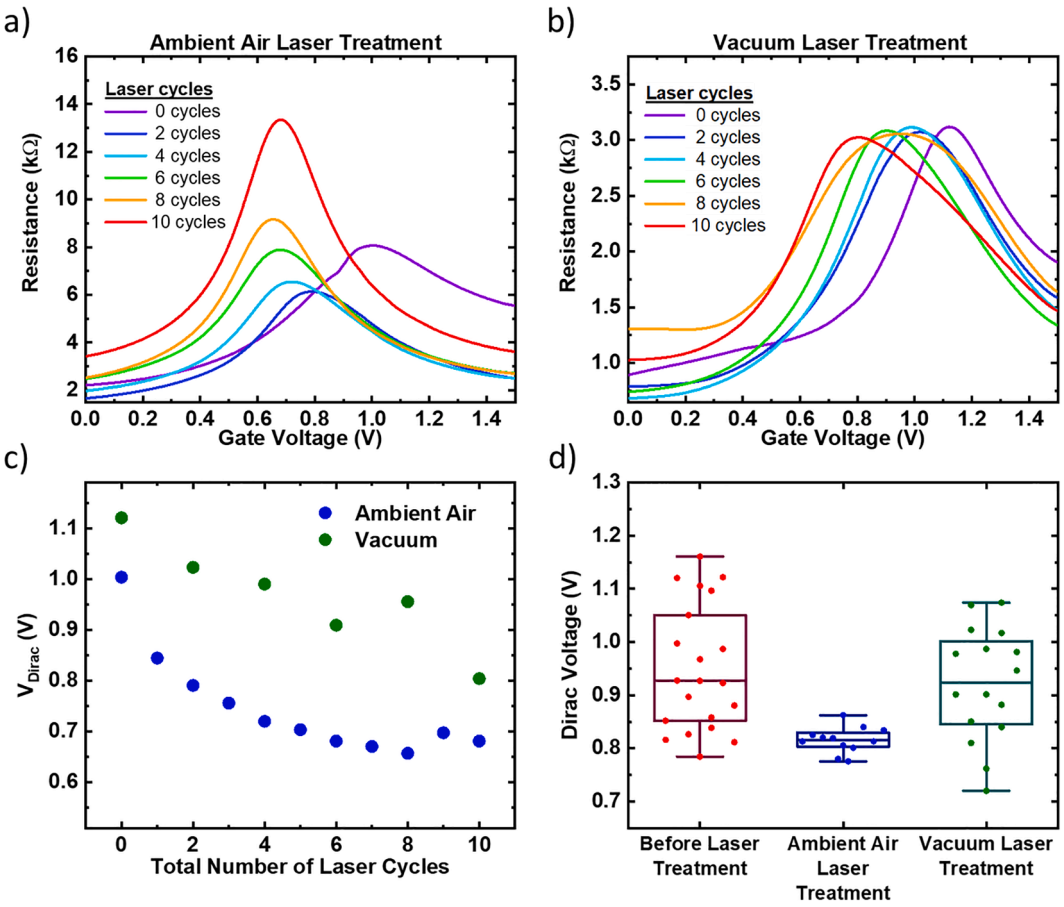

Fig. 5. Resistance versus gate voltage characteristic curves for two devices measured at different number of laser cycles. The drain source bias was set at 0.1 V. The Dirac voltage is defined as the voltage when the resistance reaches the maximum. The laser treatment was performed a) in ambient air or b) under vacuum. c) The Dirac voltage evolution, at different number of laser cycles, of the two devices measured in ambient air or under vacuum. d) The Dirac voltages distribution of a series of devices, measured without the laser treatment and with a four cycles laser treatment under the two kind of atmospheres, ambient air or vacuum.

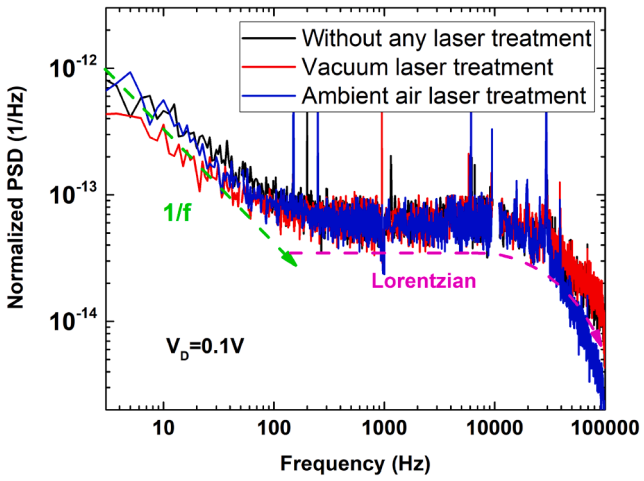

Fig. 6. Normalized power spectral density of the noise for devices before and after the laser treatment under both atmosphere conditions, in ambient air and vacuum.

the graphene-based liquid gate sensors show a reduced Dirac point and inter-device variability. These results indicate that there is a trade-off between some grade of graphene degradation and an improvement at the liquid gate/graphene interface. The structural characterization shows an increase of the sp^3 bonds in the carbon component together with an increase in the defect peak observed in the Raman spectrum. However, this defect increment also implies a shift of the Dirac voltage and an improvement of the inter-device variability. Moreover, this laser exposure does not affect the power spectral density of the current discarding an interface degradation during the device operation once the double layer is formed. Hence, the use of the laser treatment under ambient air conditions could be an advantageous technique to increase the sensibility and reproducibility of these graphene-based devices for applications as sensors or biosensors. For instance, it is planned to evaluate the sensing capabilities of these devices as biosensors. After an appropriate chemical modification of the graphene surface, these devices would be able to detect a wide variety of biomarkers. One of the main points to study in future works is to corroborate if the improved inter-device variability is maintained after the biochemical decoration. Another possibility would be the employment of simulation models to evaluate the sensing performance of the devices developed in this work.

Declaration of Competing Interest

The authors declare that they have no known competing financial interests or personal relationships that could have appeared to influence the work reported in this paper.

Acknowledgment

This work has received funding from the European Union's Horizon 2020 research and innovation programme under the Marie Skłodowska-Curie grant agreement No 895322, from the Spanish Program (DTS20/

00038 and PID2020-119668 GB-I00). SUPERA COVID-19 Fund and CRUE-Santander, Regional Program FEDER UGRVID (CV20-36685), P18-RT-4826 and A-TIC-628-UGR20 project and UGR-MADOC CEMIX 2D-EDEX are also thanked for financial support.

References

[1] Novoselov KS, Geim AK, Morozov SV, Jiang D, Zhang Y, Dubonos SV, Grigorieva IV, Firsov AA. Electric Field Effect in Atomically Thin Carbon Films. Science Oct 2004;306(5696). 666–9.

[2] A.K. Geim and K.S. Novoselov, "The rise of graphene." Nature materials, vol. 6, no. 3, pp. 183–191, 2007. [Online]. Available: url:http://www.nature.com/doifinder/10.1038/nmat1849.

[3] K.S. Novoselov, V.I. Fal ko, L. Colombo, P.R. Gellert, M.G. Schwab, and K. Kim, "A roadmap for graphene," Nature, vol. 490, no. 7419, pp. 192–200, 2012.

[4] C.W. Lee, J.M. Suh, and H.W. Jang, "Chemical Sensors Based on Two-Dimensional (2D) Materials for Selective Detection of Ions and Molecules in Liquid," Frontiers in Chemistry, vol. 7, no. November, pp. 1–21, Nov 2019. [Online]. Available: url:https://www.frontiersin.org/article/10.3389/fchem.2019.00708/full.

[5] Y. Liu, X. Dong, and P. Chen, "Biological and chemical sensors based on graphene materials," Chem. Soc. Rev., vol. 41, pp. 2283–2307, 2012. [Online]. Available: url:https://doi.org/10.1039/C1CS15270J.

[6] S. Kochmann, T. Hirsch, and O.S. Wolfbeis, "Graphenes in chemical sensors and biosensors," TrAC Trends in Analytical Chemistry, vol. 39, pp. 87–113, 2012, new Materials in Analytical Chemistry. [Online]. Available: url:https://www.sciencedirect.com/science/article/pii/S016599361200194X.

[7] M. Liu, W. Zhang, D. Chang, Q. Zhang, J.D. Brennan, and Y. Li, "Integrating graphene oxide, functional dna and nucleic-acid-manipulating strategies for amplified biosensing," TrAC Trends in Analytical Chemistry, vol. 74, pp. 120–129, 2015. [Online]. Available: url:https://www.sciencedirect.com/science/article/pii/S0165993615002253.

[8] P. Bollella, G. Fusco, C. Tortolini, G. Sanzò, G. Favero, L. Gorton, and R. Antiochia, "Beyond graphene: Electrochemical sensors and biosensors for biomarkers detection," Biosensors and Bioelectronics, vol. 89, pp. 152–166, 2017, 2D Materials in Biosensors & Bioelectronics. [Online]. Available: url:https://www.sciencedirect.com/science/article/pii/S0956566316302676.

[9] J. Chang, G. Zhou, E.R. Christensen, R. Heideman, and J. Chen, "Graphene-based sensors for detection of heavy metals in water: a review," Analytical and Bioanalytical Chemistry, vol. 406, no. 16, pp. 3957–3975, Jun. 2014. [Online]. Available: url:https://doi.org/10.1007/s00216-014-7804-x.

[10] A.T. Valota, I.A. Kinloch, K.S. Novoselov, C. Casiraghi, A. Eckmann, E.W. Hill, and R.A.W. Dryfe, "Electrochemical Behavior of Monolayer and Bilayer Graphene," ACS Nano, vol. 5, no. 11, pp. 8809–8815, Nov 2011. [Online]. Available: doi:10.1021/nn202878f.

[11] M. Dankerl, M.V. Hauf, A. Lippert, L.H. Hess, S. Birner, I.D. Sharp, A. Mahmood, P. Mallet, J.-Y. Veuillen, M. Stutzmann, and J.A. Garrido, "Graphene Solution-Gated Field-Effect Transistor Array for Sensing Applications," Advanced Functional Materials, vol. 20, no. 18, pp. 3117–3124, sep 2010. [Online]. Available: url:https://onlinelibrary.wiley.com/doi/10.1002/adfm.201000724.

[12] X. Du, H. Guo, Y. Jin, Q. Jin, and J. Zhao, "Electrochemistry Investigation on the Graphene/Electrolyte Interface," Electroanalysis, vol. 27, no. 12, pp. 2760–2765, Dec 2015. [Online]. Available: url:https://onlinelibrary.wiley.com/doi/10.1002/elan.201500302.

[13] Chen F, Qing Q, Xia J, Li J, Tao N. Electrochemical gate-controlled charge transport in graphene in ionic liquid and aqueous solution. J Am Chem Soc 2009;131(29):9908–9.

[14] N. Liu, R. Chen, and Q. Wan, "Recent advances in electric-double-layer transistors for bio-chemical sensing applications," Sensors (Switzerland), vol. 19, no. 15, 2019.

[15] A. Pirkle, J. Chan, A. Venugopal, D. Hinojos, C.W. Magnuson, S. McDonnell, L. Colombo, E.M. Vogel, R.S. Ruoff, and R.M. Wallace, "The effect of chemical residues on the physical and electrical properties of chemical vapor deposited graphene transferred to SiO 2," Applied Physics Letters, vol. 99, no. 12, p. 122108, sep 2011. [Online]. Available: url:http://aip.scitation.org/doi/10.1063/1.3643444.

[16] A. Lipatov, A. Varezhnikov, M. Augustin, M. Bruns, M. Sommer, V. Sysoev, A. Kolmakov, and A. Sinitskii, "Intrinsic device-to-device variation in graphene field-effect transistors on a si/sio2 substrate as a platform for discriminative gas sensing," Applied Physics Letters, vol. 104, no. 1, p. 013114, 2014. [Online]. Available: url:https://doi.org/10.1063/1.4861183.

[17] E. Pembroke, G. Ruan, A. Sinitskii, D.A. Corley, Z. Yan, Z. Sun, and J.M. Tour, "Effect of anchor and functional groups in functionalized graphene devices," Nano Research, vol. 6, no. 2, pp. 138–148, Feb. 2013. [Online]. Available: url:https://doi.org/10.1007/s12274-013-0289-7.

[18] B. Zhuang, S. Li, S. Li, and J. Yin, "Ways to eliminate PMMA residues on graphene superclean graphene," Carbon, vol. 173, pp. 609–636, Mar 2021. [Online]. Available: url:https://linkinghub.elsevier.com/retrieve/pii/S000862232031126X.

[19] R. You, Y.-Q. Liu, Y.-L. Hao, D.-D. Han, Y.-L. Zhang, and Z. You, "Laser fabrication of graphene-based flexible electronics," Advanced Materials, vol. 32, no. 15, p. 1901981, 2020. [Online]. Available: url:https://onlinelibrary.wiley.com/doi/abs/10.1002/adma.201901981.

[20] X.-Y. Fu, Z.-D. Chen, D.-D. Han, Y.-L. Zhang, H. Xia, and H.-B. Sun, "Laser fabrication of graphene-based supercapacitors," Photon. Res., vol. 8, no. 4, pp. 577–588, Apr 2020. [Online]. Available: url:http://www.osapublishing.org/prj/abstract.cfm?URI=prj-8-4-577.

[21] Y.-L. Zhang, J.-C. Li, H. Zhou, Y.-Q. Liu, D.-D. Han, and H.-B. Sun, "Electro-responsive actuators based on graphene," The Innovation, vol. 2, no. 4, p. 100168, 2021. [Online]. Available: url:https://www.sciencedirect.com/science/article/pii/S266667582100093X.

[22] G. Borin Barin, Y. Song, I. de Fátima Gimenez, A.G. Souza Filho, L.S. Barreto, and J. Kong, "Optimized graphene transfer: Influence of polymethylmethacrylate (PMMA) layer concentration and baking time on graphene final performance," Carbon, vol. 84, no. C, pp. 82–90, Apr 2015. [Online]. Available: url:https://linkinghub.elsevier.com/retrieve/pii/S0008622314011269.

[23] J. Chroboczek, "Automatic, wafer-level, low frequency noise measurements for the interface slow trap density evaluation," in International Conference on Microelectronic Test Structures, 2003. IEEE, 2003, pp. 95–98. [Online]. Available: url:10.1109/ICMTS.2003.1197409.

[24] A. Eckmann, A. Felten, A. Mishchenko, L. Britnell, R. Krupke, K.S. Novoselov, and C. Casiraghi, "Probing the Nature of Defects in Graphene by Raman Spectroscopy," Nano Letters, vol. 12, no. 8, pp. 3925–3930, Aug 2012. [Online]. Available: doi:10.1021/nl300901a.

[25] Huang T, Long J, Zhong M, Jiang J, Ye X, Lin Z, Li L. The effects of low power density co2 laser irradiation on graphene properties. Appl Surface Sci 2013;273:502–6.

[26] L.G. Cançado, A. Jorio, E.H.M. Ferreira, F. Stavale, C.A. Achete, R.B. Capaz, M.V.O. Moutinho, A. Lombardo, T.S. Kulmala, and A.C. Ferrari, "Quantifying defects in graphene via raman spectroscopy at different excitation energies," Nano Letters, vol. 11, no. 8, pp. 3190–3196, 2011, pMID: 21696186. [Online]. Available: url:https://doi.org/10.1021/nl201432g.

[27] A.C. Ferrari and J. Robertson, "Interpretation of raman spectra of disordered and amorphous carbon," Phys. Rev. B, vol. 61, pp. 14 095–14 107, May 2000. [Online]. Available: url:https://link.aps.org/doi/10.1103/PhysRevB.61.14095.

[28] D.L. Duong, G.H. Han, S.M. Lee, F. Gunes, E.S. Kim, S.T. Kim, H. Kim, Q.H. Ta, K.P. So, S.J. Yoon, S.J. Chae, Y.W. Jo, M.H. Park, S.H. Chae, S.C. Lim, J.Y. Choi, and Y.H. Lee, "Probing graphene grain boundaries with optical microscopy," Nature, vol. 490, no. 7419, pp. 235–239, 2012. [Online]. Available: url:https://doi.org/10.1038/nature11562.

[29] H. Ohta, Y. Sato, T. Kato, S. Kim, K. Nomura, Y. Ikuhara, and H. Hosono, "Field-induced water electrolysis switches an oxide semiconductor from an insulator to a metal," Nature Communications, vol. 1, no. 8, 2010.

[30] B. Standley, A. Mendez, E. Schmidgall, and M. Bockrath, "Graphene–Graphite Oxide Field-Effect Transistors," Nano Letters, vol. 12, no. 3, pp. 1165–1169, Mar 2012. [Online]. Available: doi:10.1021/nl2028415.

[31] Y. Yang and R. Murali, "Binding mechanisms of molecular oxygen and moisture to graphene," Applied Physics Letters, vol. 98, no. 9, p. 093116, Feb 2011. [Online]. Available: url:http://aip.scitation.org/doi/10.1063/1.3562317.

[32] T.A. Oproglidis, T.A. Karatsori, C.G. Theodorou, D. Tassis, S. Barraud, G. Ghibaudo, and C.A. Dimitriadis, "Origin of Low-Frequency Noise in Triple-Gate Junctionless n-MOSFETs," IEEE Transactions on Electron Devices, vol. 65, no. 12, pp. 5481–5486, Dec 2018. [Online]. Available: url:https://ieeexplore.ieee.org/document/8494709/.